Local detection efficiency of a NbN superconducting single photon detector explored by a scattering scanning near-field optical microscope

Wang, Qiang ; Renema, Jelmer J ; Engel, Andreas ; van Exter, Martin P ; de Dood, Michiel J A

DOI: https://doi.org/10.1364/OE.23.024873

Local detection efficiency of a NbN superconducting single photon detector explored by a scattering scanning near-field optical microscope

Qiang Wang,[1,*] Jelmer J. Renema,[1] Andreas Engel,[2] Martin P. van Exter,[1] and Michiel J. A. de Dood[1]

[1]*Huygens Kamerlingh-Onnes Laboratory, Leiden University, Niels Bohrweg 2, 2333 CA Leiden, The Netherlands*

[2]*Physics Institute of the University of Zurich, Winterthurerstr. 190, 8057 Zurich, Switzerland*

[*]*wang@physics.leidenuniv.nl*

Abstract: We propose an experiment to directly probe the local response of a superconducting single photon detector using a sharp metal tip in a scattering scanning near-field optical microscope. The optical absorption is obtained by simulating the tip-detector system, where the tip-detector is illuminated from the side, with the tip functioning as an optical antenna. The local detection efficiency is calculated by considering the recently introduced position-dependent threshold current in the detector. The calculated response for a 150 nm wide detector shows a peak close to the edge that can be spatially resolved with an estimated resolution of $\sim$ 20 nm, using a tip with parameters that are experimentally accessible.

OCIS codes: (040.5570) Quantum detectors; (180.4243) Near-field microscopy; (230.0040) Detectors.

References and links

1. P. Anger, P. Bharadwaj, and L. Novotny, "Enhancement and quenching of single-molecule fluorescence," Phys. Rev. Lett. **96**, 113002 (2006).
2. R. B. G. de Hollander, N. F. van Hulst, and R. P. H. Kooyman,"Near field plasmon and force microscopy," Ultramicroscopy **57**, 263–269 (1995).
3. J. Chen, M. Badioli, P. Alonso-Gonzalez, S. Thongrattanasiri, F. Huth, J. Osmond, M. Spasenovic, A. Centeno, A. Pesquera, P. Godignon, A. Z. Elorza, N. Camara, F. Javier Garca de Abajo, R. Hillenbrand, and F. H. L. Koppens, "Optical nano-imaging of gate-tunable graphene plasmons," Nature **487**, 77–81 (2012).
4. Q. Wang, and M. J. A. de Dood, "An absorption-based superconducting nano-detector as a near-field optical probe," Opt. Express **21**, 3682–3692 (2013).
5. R. H. Hadfield, P. A. Dalgarno, J. A. O'Connor, E. Ramsay, R. J. Warburton, E. J. Gansen, B. Baek, M. J. Stevens, R. P. Mirin, and S. W. Nam, "Submicrometer photoresponse mapping of nanowire superconducting single-photon detectors," Appl. Phys. Lett. **91**, 241108 (2007).
6. J. A. O'Connor, M. G. Tanner, C. M. Natarajan, G. S. Buller, R. J. Warburton, S. Miki, Z. Wang, S. W. Nam, and R. H. Hadfield, "Spatial dependence of output pulse delay in a niobium nitride nanowire superconducting single-photon detector," Appl. Phys. Lett. **98**, 201116 (2011).
7. J. J. Renema, Q. Wang, R. Gaudio, I. Komen, K. op 't Hoog, D. Sahin, A. Schilling, M. P. van Exter, A. Fiore, A. Engel, and M. J. A. de Dood, "Position-dependent local detection efficiency in a nanowire superconducting single-photon detector," Nano Lett. **15**, 4541–4545 (2015)
8. A. Engel, J. Lonsky, X. Zhang, and A. Schilling, "Detection mechanism in SNSPD: numerical results of a conceptually simple, yet powerful detection model," IEEE Trans. Appl. Supercon. **25**, 2200407 (2015).

#242194 Received 3 Jun 2015; revised 28 Aug 2015; accepted 2 Sep 2015; published 14 Sep 2015

9. F. Marsili, V. B. Verma, J. A. Stern, S. Harrington, A. E. Lita, T. Gerrits, I. Vayshenker, B. Baek, M. D. Shaw, R. P. Mirin, and S. W. Nam, "Detecting single infrared photons with 93% system efficiency," Nat. Photonics **7**, 210–214 (2013).
10. E. F. C. Driessen, F. R. Braakman, E. M. Reiger, S. N. Dorenbos, V. Zwiller, and M. J. A. de Dood, "Impedance model for the polarization-dependent optical absorption of superconducting single-photon detectors," Eur. Phys. J. Appl. Phys. **47**, 10701–10706 (2009).
11. V. Anant, A. J. Kerman, E. A. Dauler, J. K. W. Yang, K. M. Rosfjord, and K. K. Berggren, "Optical properties of superconducting nanowire single-photon detectors," Opt. Express **16**, 10750–10761 (2008).
12. A. J. Kerman, E. A. Dauler, W. E. Keicher, J. K. W. Yang, K. K. Berggren, G. Gol'tsman, and B. Voronov, "Kinetic-inductance-limited reset time of superconducting nanowire photon counters," Appl. Phys. Lett. **88**, 111116 (2006).
13. J. J. Renema, R. Gaudio, Q. Wang, Z. Zhou, A. Gaggero, F. Mattioli, R. Leoni, D. Sahin, M. J. A. de Dood, A. Fiore, and M. P. van Exter, "Experimental test of theories of the detection mechanism in a nanowire superconducting single photon detector," Phys. Rev. Lett. **112**, 117604 (2014).
14. L. N. Bulaevskii, Matthias J. Graf, and V. G. Kogan, "Vortex-assisted photon counts and their magnetic field dependence in single-photon superconducting detectors," Phys. Rev. B **85**, 014505 (2012).
15. B. Knoll, and F. Keilmann, "Enhanced dielectric contrast in scattering-type scanning near-field optical microscopy," Opt. Commun. **182**, 321–328 (2000).
16. Rsoft Version 8.1.0.0.7, http://optics.synopsys.com/rsoft/
17. J. J. Renema, G. Frucci, Z. Zhou, F. Mattioli, A. Gaggero, R. Leoni, M. J. A. de Dood, A. Fiore, and M. P. van Exter, "Universal response curve for nanowire superconducting single-photon detectors," Phys. Rev. B **87**, 174526 (2013).
18. J. R. Clem, and K. K. Berggren, "Geometry-dependent critical currents in superconducting nanocircuits," Phys. Rev. B **84**, 174510 (2011).
19. H. L. Hortensius, E. F. C. Driessen, T. M. Klapwijk, K. K. Berggren, and J. R. Clem, "Critical-current reduction in thin superconducting wires due to current crowding," Appl. Phys. Lett. **100**, 182602 (2012).
20. A. D. Rakic, A. B. Djurišic, J. M. Elazar, and M. L. Majewski, "Optical properties of metallic films for vertical-cavity optoelectronic devices," Appl. Opt. **37**, 5271–5283 (1998)
21. K. Tanabe, H. Asano, Y. Katoh, and O. Michikami, "Ellipsometric and optical reflectivity studies of reactively sputtered NbN thin films," J. Appl. Phys. **63**, 1733–1739 (1988)
22. E. F. C. Driessen, and M. J. A. de Dood, "The perfect absorber," Appl. Phys. Lett. **94**, 171109 (2009).
23. D. Lim, K. Jeon, J. Hwang, H. Kim, Su. Kwon, Y. Suh, and J. Nam, "Highly uniform and reproducible surface-enhanced Raman scattering from DNA-tailorable nanoparticles with 1-nm interior gap," Nat. Nano **6**, 452–460 (2011).
24. R. W. Taylor, T. Lee, O. A. Scherman, R. Esteban, J. Aizpurua, F. Huang, J. J. Baumberg, and S. Mahajan, "Precise subnanometer plasmonic junctions for sers within gold nanoparticle assemblies using cucurbit[n]uril 'glue'," ACS Nano **5**, 3878–3887 (2011).
25. R. Esteban, A. G. Borisov, P. Nordlander, and J. Aizpurua, "Bridging quantum and classical plasmonics with a quantum-corrected model," Nat. Commun. **3**, 825 (2012).
26. L. Novotny, R. X. Bian, and X. Sunney Xie, "Theory of nanometric optical tweezers," Phys. Rev. Lett. **79**, 645–648 (1997).
27. A typical simulation involves 3×10^6 grid points and 1.8×10^4 time steps and takes approximately 400 minutes to complete on a PC (Intel Xeon E5420, 2.54 GHz, 16.0 GB RAM).
28. Q. Wang, and M. J. A. de Dood, "Near-field single-photon detection in a scattering SNOM," Proc. SPIE 9504, 950403 (2015).
29. N. Behr, and M. B. Raschke, "Optical antenna properties of scanning probe tips: plasmonic light scattering, tip-sample coupling, and near-field enhancement," J. Phys. Chem. C **112**, 3766–3773 (2008).
30. F. Huth, A. Chuvilin, M. Schnell, I. Amenabar, R. Krutokhvostov, S. Lopatin, and R. Hillenbrand, "Resonant antenna probes for tip-enhanced infrared near-field microscopy," Nano Lett. **13**, 1065–1072 (2013)
31. J. J. Bowman, T. B. A. Senior, and P. L. E. Uslenghi, *Electromagnetic and Acoustic Scattering by simple Shapes* (North-Holland, 1969).
32. A. V. Goncharenko, M. M. Dvoynenko, H. Chang, and J. Wang, "Electric field enhancement by a nanometer-scaled conical metal tip in the context of scattering-type near-field optical microscopy," Appl. Phys. Lett. **88**, 104101 (2006).
33. J. I. Gersten, "The effect of surface-roughness on surface enhanced Raman scattering," J. Chem. Phys. **72**, 5779–5780 (1980).
34. J. D. Jackson, "Radiating systems, multipole fields and radiation," in *Classical Electrodynamics* (Wiley & Sons, 1983).
35. Z. Yang, J. Aizpurua, and H. Xu, "Electromagnetic field enhancement in TERS configurations," J. Raman Spectrosc. **40**, 1343–1348 (2009).
36. J. D. Jackson, "Maxwell equations, macroscopic electromagnetism, conservation laws," in *Classical Electrodynamics* (Wiley & Sons, 1983).

#242194 Received 3 Jun 2015; revised 28 Aug 2015; accepted 2 Sep 2015; published 14 Sep 2015

37. R. HillenbRand, B. Knoll, and F. Keilmann, "Pure optical contrast in scattering-type scanning near-field microscopyJournal of Microscopy," J. Microsc. **202**, 77–83 (2001).
38. T. Taubner, R. Hillenbrand, and F. Keilmann, "Performance of visible and mid-infrared scattering-type near-field optical microscopes," J. Microsc. **210**, 311–314 (2003).
39. J. D. Jackson, "Boundary-value problems in electrostatics: II," in *Classical Electrodynamics* (Wiley & Sons, 1983).

1. Introduction

Scanning near-field optical microscopes (SNOMs) beat the diffraction-limit of conventional optical microscopes and are able to probe nanoscale structures such as single molecules [1], plasmonic antennas [2] or graphene [3], by scattering part of the optical near field via a sharp tip (scattering-SNOM or s-SNOM) or a metal coated fiber (aperture-SNOM or a-SNOM) to a photon sensitive detector placed in the optical far field. However, the signal collection in SNOMs is extremely inefficient, because the Rayleigh scattering process between the sample and the subwavlength apex of the tip or the fiber has a scattering cross section proportional to a^6/λ^4, where a is the size of the apex. Typical values of a are $\sim 1/10$ to $1/50$ of the incident wavelength λ. The low efficiency limits the application of SNOM in quantum optics, which requires very high signal collection efficiency. Our previous work [4] shows a highly efficient near-field probe made out of a nanoscale NbN superconducting single photon detector (SSPD), which gives two orders of magnitude higher absorbtion compared to a conventional SNOM.

According to the calculation of optical absorption in [4], the spatial resolution of the nano SSPD under the illumination of a point light source (a radiative electric dipole) is estimated to be approximately equal to the dimension of the nano SSPD. Studies on the spatial dependence of the response of SSPD on a micrometer or sub-micrometer scale have been reported [5, 6]. Recent experiments [7] and modeling [8] of SSPDs show that the response of the SSPDs consist of not only the optical absorption but also the internal detection efficiency that is related to the intrinsic detection process. Hence, the spatial resolution of the SSPD is not trivial, and contains information about the intrinsic photon-detection process and is worthy of being investigated for applications in optical near-field microscopy. Moreover, these detectors are technologically interesting because the very thin and narrow wire can be used to detect single photons over a broad wavelength range with minimal timing jitter, small detector dead-time and high system detection efficiency [9].

In this article we use a short metallic tip in an s-SNOM to investigate the local response of a strongly absorbing SSPD, which is based on the fact that the sharp tip can localize the illuminated light field and act as a point-like light source to probe the SSPD in the optical near field. When the superconducting nanowire is biased close to its critical current, absorption of a single photon can induce a transition from the superconducting to the normal state. This transition leads to a voltage difference that can be amplified to create a measurable signal.

Three steps are needed to understand the photon detection process in SSPDs: the photon absorption [10, 11], the generation of the voltage pulse and the self-resetting mechanism [12]. The initial and final steps are well-understood. Recently, significant progress has also been made in the understanding of the intermediate step [8, 13, 14] where the absorbed photon leads to a transition of a cross section of the wire to the normal state that leads to the voltage pulse. Experimental results for visible to near-infrared wavelengths absorbed by a short NbN nanowire confirm predictions from a photon-assisted vortex entry model [8]. In this model, photon absorption leads to a decrease of the locally available Cooper pairs that carry the current in the superconductor. The initial excitation diffuses in the superconductor without breaking superconductivity and lowers the edge barrier for vortex entry. If this barrier is lowered enough, a magnetic vortex transits the wire cross section and dissipates additional energy that triggers the detector. A direct consequence of the photon-assisted vortex entry model is that the absorption

#242194 Received 3 Jun 2015; revised 28 Aug 2015; accepted 2 Sep 2015; published 14 Sep 2015

of a photon near the edge of the wire is more efficient than absorption in the center, because this directly affects the redistribution of supercurrent at the edge.

A local detection efficiency $LDE(x)$ can describe the position dependent detector response [7]. The typical length scale over which this $LDE(x)$ can vary is set by diffusion of electrons from the position of initial excitation, which is about 10 - 30 nm. Further experiments are needed that either measure this size or that explore the dynamics of electrons and quasiparticles in a NbN nanowire. A conventional a-SNOM based on a scanning aperture is typically limited by the skin-depth of the metal used to create the aperture. Even for good conductive metals, such as gold, this limits the resolution to $\geq$ 20 - 50 nm. Therefore, we explore the possibility to use an s-SNOM to probe a NbN nanowire with a spatial resolution comparable to 10 nm, using the calculated position dependent response [8] of the detector as a reference.

It remains an open question, if the s-SNOM technique can be applied successfully to strongly absorbing structures such as the NbN nanowire considered here. The resolution and sensitivity of s-SNOM is determined by the shape and resonant nature of the tip that strongly enhances the field at the tip vertex. In the presence of a good metal or low loss dielectric substrate the tip-sample interaction can be understood via an image dipole of the tip in the substrate [15]. Because the losses are minimal, the resonant enhancement of the field that is critical to the operation of the s-SNOM is not negatively influenced by the substrate. This situation drastically changes when the resonant nature of the tip is damped by a strongly absorbing sample in the near field. To explore the effect of the detector on the tip resonance and to evaluate the performance of the proposed scanning probe we perform numerical finite-difference-time-domain (FDTD) calculations that we combine with a model of the photon detection process in order to simulate the complete response of the superconducting detector.

2. Simulation configuration

We calculate the optical response of a superconducting single photon detector in an s-SNOM via the FDTD method [16]. Figure 1 shows the geometry of the NbN single nanowire (100 nm long, 150 nm wide and 5nm thick) in between two tapered parts on a semi-infinite GaAs substrate. The NbN single nanowire has dimensions identical to a device that has been studied experimentally [7, 17]. This simple design avoids the problem of current-crowding that occurs in the bends of meandering structures that are usually used in SSPDs [18, 19].

In the experiment that we simulate, the detector placed in a cryostat is cooled below its critical temperature ($\sim$ 10 K), and is biased with a current I_b, close to the critical current I_c. Absorption of the energy of a single photon can drive the nanowire from the superconducting state to the normal state with some internal probability. Once the wire is in a resistive state a voltage difference over the wire is generated that can be amplified and read out with pulse counting electronics.

The dielectric constants of GaAs and gold are taken from RSoft Library [16] and [20], respectively. The dielectric constant ε_{NbN} of NbN is described by a Drude model [21], which makes NbN a metal-like material but with strong absorption or Ohmic loss due to the large imaginary part of ε_{NbN} [22].

Figure 2 shows the configuration of the s-SNOM with a gold tip in the shape of a rounded cone above the detector. The gap between the tip and the nanowire is set to 5 nm, because this distance ensures that the detector is within the near field of the tip, while avoiding problems of electron tunneling [23–25]. For example, at sub-nanometric scale ($\sim$ 5Å) the electronic densities of the individual sub-nanostructures tend to overlap and the field enhancements of the resonant modes cannot be described by a classical description, and quantum effects need to be accounted for [25].

The incident light illuminates the detector and tip from the side and has a wave-vector k that is

#242194 Received 3 Jun 2015; revised 28 Aug 2015; accepted 2 Sep 2015; published 14 Sep 2015

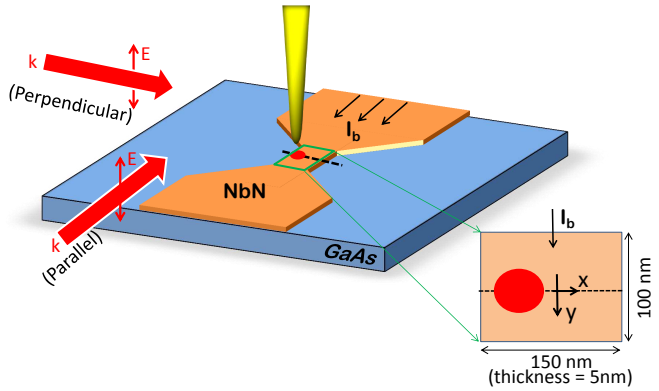

Fig. 1. Schematic diagram of the tip-detector system in a scattering SNOM considered in the simulation. A 5 nm thick NbN film on a GaAs substrate is patterned into a short wire in between two tapered parts. Only the central part of the wire with a width of 150 nm and a length of 100 nm is considered in the simulation. A rounded and conical gold tip is positioned above the detector with a fixed height of 5 nm and scanned in either x- or y-direction. The tip-detector system is illuminated by a plane wave with a wave-vector k either parallel or perpendicular to the single wire. The incident field is polarized with the electric field along (parallel to) the long axis of the tip. The simulation area is 200 nm by 200 nm by 250 nm in the x, y and z-directions with a Perfectly Matched Layer at the boundaries.

either parallel or perpendicular to the wire. The polarization of the incident light is kept constant with its electric field parallel to the long axis of the tip, which leads to a strong electric field enhancement at the tip. For this polarization the induced surface charge density is symmetric about the long axis of the tip and has the highest amplitude at the end of the tip, leading to a large enhancement of the local electric field. For an electric field perpendicular to the tip the surface charge is distributed diametrically at opposed points on the tip, and very little charge is accumulated at the apex of the tip, and the enhancement of the electric field is negligible [26].

To reduce the computational time for 3D FDTD calculation [27], we concentrate on the central nanowire of the detector, namely the active area shown as the magnified section in Fig. 1. The considered nanowire has a size of 150 nm (width, x-direction) by 100 nm (length, y-direction) by 5 nm (thickness, z-direction), and the entire simulation area is 200 nm (x-direction) by 200 nm (y-direction) by 250 nm (z-direction). At the boundaries a Perfectly Matched Layer (PML) with thickness of 50 nm and reflection of 10^{-12} is added. The spacing of grid points is set to 0.25 nm on the boundary of the NbN film and to 0.5 nm inside the film.

Limiting the simulation to the central part is justified because the localized electric field area given by the tip is confined to an area ~ 50 nm compared to the 100 nm long wire of the detector in the simulation. The 'contacts' or the tapered parts have little influence on the electric field distribution in the central nanowire [7], because the NbN material does not support surface plasmons modes due to the strong damping. This eliminates the capacitive coupling between the tapers that is responsible for the resonance in antennas made from more plasmonic metals such as Au or Ag. The simulation volume used in this work is sufficient to answer the main physical questions we are interested in. We have tested the stability of the FDTD with a simple model of a stratified, 5 nm thick, NbN film and find that the simulated optical properties deviate less than 1.5% from the analytical solution.

#242194 Received 3 Jun 2015; revised 28 Aug 2015; accepted 2 Sep 2015; published 14 Sep 2015

The simplified settings make simulation of a single configuration possible within a reasonable amount of time ($\sim$ 7 hours). The optical absorption of the nanowire is recorded and analyzed.

3. Enhanced electric field and absorption

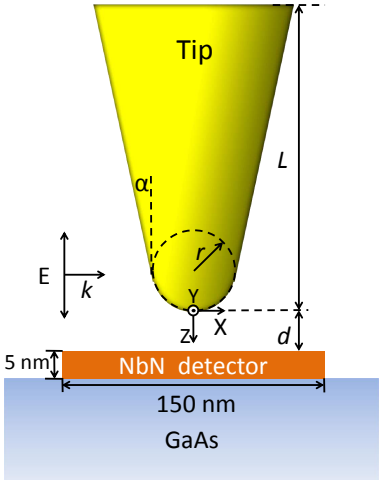

Fig. 2. Cross section of the 3D model with the tip above the center of the detector. The geometry of the tip is set in the way of $\alpha = 15°$, r = 10 nm, and L = 200 nm. The central nanowire of the NbN detector is 150 nm wide and 5 nm thick on a semi-infinite GaAs substrate. The gap d between the tip and the detector is fixed to 5 nm. The polarization of the incident light is parallel to the long axis of the tip. The origin of the coordinates is placed at the bottom of the tip and its z-axis points to the nanowire.

Figure 2 shows the detailed geometry of the gold tip. The origin of the coordinates is set at the bottom of the tip with the positive z-axis pointing to the detector. The tip is modeled as a combination of a cone (semi-angle $\alpha = 15°$ and length L = 200 nm) and a hemisphere (radius r = 10 nm) at the end. The parameters of the tip are chosen as a realistic design amendable to fabrication. More detailed information about how each of the geometric parameters (α, L, r) influences the absorption in the detector is included in [28].

As a rule of thumb, the sharp tip serves as an antenna which localizes the electric field into a limited area within a range of $2r$ from the end of the tip [29]. Hence, the gap d between the tip and the nanowire is fixed to 5 nm, to place the detector in the area of enhanced electric field.

Figure 3 shows the absorption cross section of the NbN detector with tip as a function of wavelength to illustrate the resonant enhancement of the absorption by the tip. To calculate the wavelength dependence, we use a well defined pulse with a Gaussian envelope function with a width of 2.67 fs, which multiplies a sinusoidal carrier wave with a center wavelength of 800 nm [16].

The horizontal dashed line in Fig. 3 indicates the 100×150 nm^2 geometric area of the nanowire, as a reference. The inset of Fig. 3 demonstrates the relative permittivity of NbN based on the Drude model [21]. The imaginary part, which dominantly determines the absorption in the nanowire, increases monotonically with wavelength. This agrees well with the trend of the absorption increase of the nanowire without tip (black dashed line in Fig. 3). The solid curves are calculations of the absorption cross section of the nanowire in the presence of a tip

#242194 Received 3 Jun 2015; revised 28 Aug 2015; accepted 2 Sep 2015; published 14 Sep 2015

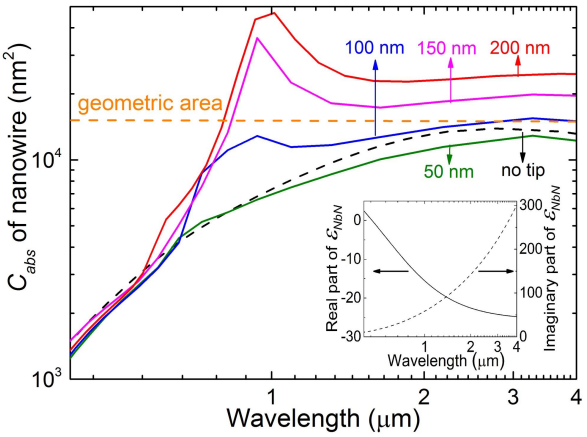

Fig. 3. Calculated absorption cross section C_{abs} of the nanowire as a function of wavelength in the presence of a tip of varying length. The black dashed line is the absorption of the nanowire without tip and the colored curves are with tips of different lengths from 50 nm to 200 nm. As a reference, the horizontal dashed line shows the geometry area of the 100×150 nm^2 nanowire. The real and imaginary parts of the relative permittivity of NbN are shown in the inset.

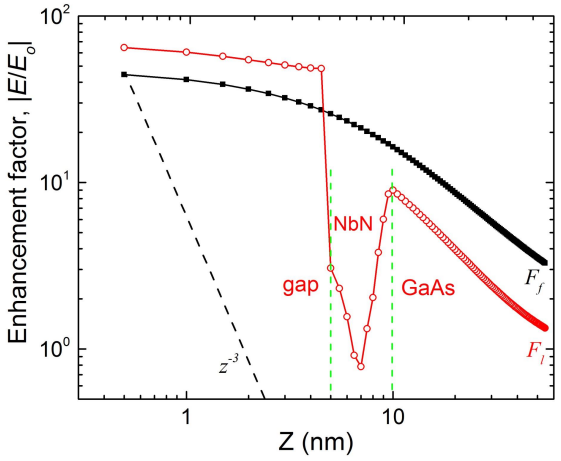

Fig. 4. Simulations of the electric field enhancement of a gold tip close to the nanowire along the long axis of the tip (z-axis). The black squares (F_f) are the field enhancement of a bare tip without nanowire and substrate, and it is fitted to the sharp cone model (black curve). The red dots (F_l) are the calculated field enhancement in the presence of the nanowire and the substrate. For comparison the dashed line shows the behavior of z^{-3} for the field enhancement in the near field of a radiative dipole. Two green vertical dashed lines separate the red dots into three regions: the 'gap' region (5 nm) between the tip and nanowire, the 'NbN' film region, and the 'GaAs' substrate region.

#242194 Received 3 Jun 2015; revised 28 Aug 2015; accepted 2 Sep 2015; published 14 Sep 2015

with varying lengths from 50 nm to 200 nm (the curvature radius and the semi-angle of the tip are kept constant). The length of the tip determines the resonance condition for surface plasmons along the tip and causes the resonance to shift to the blue as the tip becomes shorter [30]. From these calculations we observe that for a tip length of 200 nm the absorption is about one order of magnitude higher than that without tip at the resonant wavelength of ~ 1000 nm. This peak originates from the fundamental mode of the surface plasmon resonance in the tip. A feature can be distinguished in the shoulder of the main resonance around a wavelength of 650 nm that we attribute to the second order mode of the surface plasmon standing wave along the tip [26, 30].

In order to better understand the enhancement of the detector absorption, we calculate the electric field of the tip-detector system for a constant wavelength of 1000 nm, close to the resonance in absorption. We introduce an enhancement factor $F = |E/E_o|$, where E is the total electric field in the presence of the tip and E_o is the incident electric field. We simulate the enhancement factor F_f for the 'free tip' by considering a bare tip in vacuum without nanowire and substrate, as well as the factor F_l for the 'loaded tip' for the configuration depicted in Fig. 2. Figure 4 shows the enhancement as a function of position along the z-axis where $z = 0$ corresponds to the end of the tip. The black and red colors stand for F_f in vacuum and F_l in the presence of the nanowire and substrate, respectively.

As can be seen, the enhancement F_f is largest close to the tip and decreases away from the end of the tip. To understand the F_f, we fit the black dots to a model of a sharp, perfect-conductive cone with an expression of $F_f(z) = F_o(1+z/z_o)^{\nu-1}$ [31,32], where $F_o = F(z=0) = 48.5 \pm 0.2$, $z_o = 8.7 \pm 0.2$ nm and $\nu = -0.42 \pm 0.01$. The value of the parameter ν is determined by the semi-angle α of the tip [31].

For an infinite, perfect-conductive and sharp cone, its localized electric field is expressed by $E(z) \propto z^{\nu-1}$ with $0 < \nu < 1$ [31], and contains only contributions from the lightning rod effect [33], because the surface plasmon resonance mode does not exist along a tip with an infinite length. For pure electric dipole radiation caused by a surface plasmon resonance, the decay of F_f should show a z^{-3} ($\nu = -2$) behavior (dashed line in Fig. 4) [34].

In our calculation for a finite and rounded cone the fitting parameter $\nu = -0.42 \pm 0.1$ is between the two extreme cases. This indicates a combination of the two mechanisms: the local resonance of surface electron oscillation (surface plasmon) and the local field increase due to curvature (lightning rod effect).

With the nanowire and substrate the F_l becomes complicated. As shown in Fig. 4, the F_l (red dots) has three parts, divided by two vertical dashed lines. The first part corresponds to the vacuum 'gap' region between the tip and the nanowire. The F_l of this region is higher ($50 - 65$) than that of the vacuum case ($27 - 45$) (black squares). The difference is due to reflection of the field by the nanowire that constructively interferes with light scattered by the tip [35].

The middle part, where the 5 nm thick NbN film lies, has a very low F_l caused by the very lossy nature of NbN. The relative permittivity of NbN is set to $\varepsilon_{NbN} = -15.57 + 58.62i$ according to the Drude model, where the large imaginary part makes it very lossy. Because of this it is hard for electrons in the NbN film to be driven by the external field, leading to a weak electric field and a low F_l consequently. For the F_l in the GaAs substrate the electric field penetrating into the substrate is relative low due to the large dielectric constant of the GaAs $\varepsilon_{GaAs} = 12.25$.

In our calculation we choose a simple setting of a 200 nm long tip without any support for simplicity. In practice the tip can be fabricated on a silicon pillar [30]. We perform additional simulations for the tip with a silicon support (not shown here), that show that the resonance of the tip is broadened and redshifted, because the support on one end of the tip functions as a load. This lowers the surface plasmon resonance quality factor and induces a redshift [28]. The absorption area remains within 50 nm. This can be explained because at the other end of the tip,

#242194 Received 3 Jun 2015; revised 28 Aug 2015; accepted 2 Sep 2015; published 14 Sep 2015

the localization of the electric field originates from both the surface plasmon resonance and the lightning rod effect. The latter effect is determined by the unchanged semi-angel and the radius of the tip. Therefore we expect that a tip with support will lead to very similar conclusions.

4. Position-dependent absorption and local detection efficiency

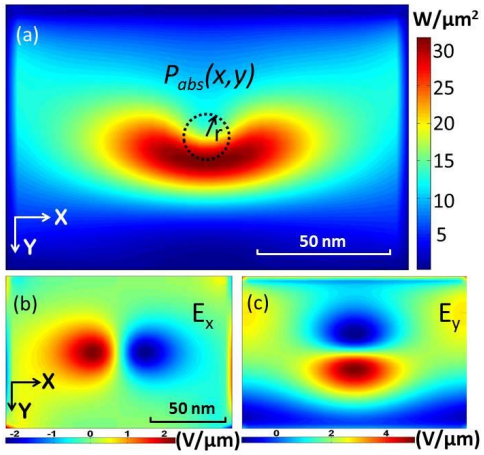

Fig. 5. The position dependent time-averaged absorbed power $P_{abs}(x,y)$ for a tip centered at $x_{tip} = y_{tip} = 0$ with the total illumination power of 1 W(a). The tip is located above the center of the nanowire and illuminated by light incident from the positive y-direction. The central part is circled in dashed curve with the radius of the tip curvature r = 10 nm. Electrical field components E_x (b) and E_y (c) in the 150 nm × 100 nm nanowire demonstrating the radiative electrical dipole nature of the tip. Components E_x and E_y are displayed at the moment of maximum amplitude contrast in the lobes that oscillate out of phase.

There are two factors that together determine the efficiency of a detection event in the detector: the spatial distribution of optical absorption and the local detection efficiency $LDE(x)$. The optical absorption over the detector corresponds to the fraction of light (or probability of a photon) absorbed in the active area (nanowire) of the detector, and the local detection efficiency quantifies the probability for the absorbed light (or photons) to trigger the detector.

To model these two effects, we assume that the overall detection efficiency or the normalized photon count rate R can be expressed as follows:

$$R(x_{tip}, I_b) = \int\int A(x_{tip}, x, y) * LDE(x, I_b) dxdy \tag{1}$$

where $A(x_{tip}, x, y)$(in unit of μm^{-2}) is the optical absorption distribution in the x-y plane of the nanowire with the tip at a position x_{tip} and $LDE(x, I_b)$ is the local detection efficiency across the nanowire, which is assumed to depend on position and bias current at a constant photon energy (wavelength). In our calculation we keep y_{tip} = 0 and the gap d = 5 nm constant, to focus our attention to an experiment where the tip is scanned in a direction across the nanowire. We will discuss the details of these two factors separately.

The absorption distribution $A(x,y)$ with the tip at x_{tip} is expressed as follows [36]:

$$A(x_{tip}, x, y) = \frac{P_{abs}(x_{tip}, x, y)}{P_{total}} = \frac{\int_0^t \frac{1}{2}\omega\varepsilon_o \text{Im}(\varepsilon_{NbN})|E(x_{tip}, x, y, z)|^2 dz}{P_{total}}, \tag{2}$$

#242194 Received 3 Jun 2015; revised 28 Aug 2015; accepted 2 Sep 2015; published 14 Sep 2015

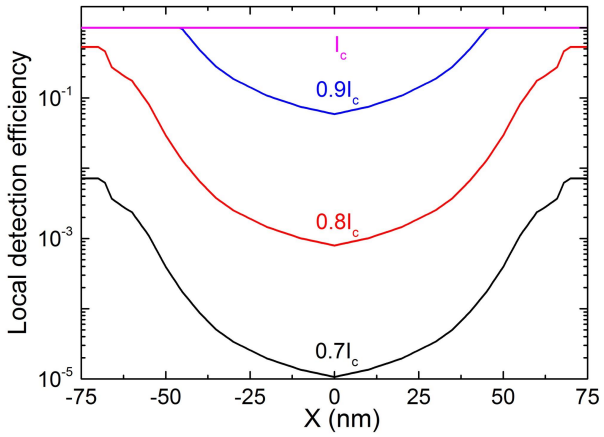

Fig. 6. Local detection efficiency across the nanowire. The detection efficiency is calculated at bias currents of $0.7I_c$, $0.8I_c$, $0.9I_c$ and I_c according to Eq. (3).

where P_{total} is the total illumination power, $P_{abs}(x,y)$ (in unit of $\mathrm{W}\mu\mathrm{m}^{-2}$) is the absorbed power density in x-y plane, ω is the frequency of the incident light, ε_o is vacuum permittivity, t = 5 nm is the thickness of the NbN film, and $|E(x_{tip},x,y,z)|^2 = |E_x|^2 + |E_y|^2 + |E_z|^2$.

In Eq. (1) the absorption distribution is independent of z and simplified by the integral of Eq. (2). This approximation is reasonable since the 5 nm thick NbN film is much thinner than the skin depth of $\sim$ 70 nm at the relevant wavelength of 1000 nm. The absorption is uniform over the thickness of the film. Figure 5 shows the absorbed power $P_{abs}(x_{tip},x,y)$ (a) and electric field components E_x (b) and E_y (c) in the nanowire with the total illumination power P_{total} = 1 W. In this simulation the tip is above the center of the wire ($x_{tip} = y_{tip} = 0$) and the wave vector of the incident light (monochromatic Gaussian beam) is pointing in the negative y-direction. As can be seen in the figure, the absorption is concentrated within a 50 nm area of the central part of the nanowire, as a result of the strongly localized electric field of the tip. The localized absorption area is asymmetric, because the illumination direction is along the y-axis, and part of the light is reflected back by the metal tip.

In order to understand the shape of the absorption distribution, we plot the position-dependent components E_x and E_y of the electric field in Fig. 5(b) and 5(c), respectively. E_x displays a pair of lobes that oscillate out of phase. The field pattern E_y shows a more complicated oscillation with multiple lobes, and the amplitude of the bottom lobe (red) is higher than that of top one (blue), as a consequence of the asymmetry of the absorption area. $|E_z|$ (not shown) is isotropic with its maximum value in the center. All these components are typical features of a radiative electric dipole, originating from the surface plasmon oscillation excited by the external field.

The results for illumination along the x-axis are similar, with the absorption pattern in Fig. 5(a) rotated by 90° clockwise. This proves that the electric field is strongly concentrated at the tip (within $\sim$ 50 nm) and is not influenced by the edges of the nanowire or the tapered parts at the two ends when the tip is located above the center of the nanowire.

In order to calculate the local detection efficiency $LDE(x,I_b)$ we consider the photon-assisted vortex entry model in [8] and the experimental results in [7]. According to this model the absorbed photon excites one electron in the NbN film. The electron thermalizes via inelastic scattering with other electrons, Cooper-pairs and the lattice, generating a localized cloud of

#242194 Received 3 Jun 2015; revised 28 Aug 2015; accepted 2 Sep 2015; published 14 Sep 2015

quasi-particles. This cloud of quasi-particles diffuses and leads to the local decrease of the superconducting electron density. Consequently, the vortex pinned at the edge of the nanowire has an increased possibility to enter the nanowire due to the decrease of the barrier potential. The energy dissipation of this moving vortex triggers a detection event.

A distinctive feature of such a model is that photon absorption at the edge is more likely to lead to a photon detection. An absorption event at the edge of the wire reduces the current density at the edge due to the reduction in the number of superconducting electrons, which slightly increases the barrier potential. However, this is more than compensated by the reduction of the vortex self-energy, which is proportional to the density of the superconducting electrons. The overall effect is that the total barrier for vortex entry is lowered. Therefore, vortices enter more easily when the superconductivity is weakened at their entry point, and that makes the detector more efficient at the edges. A position-dependent threshold current $I_{th}(x)$ is sufficient to quantify this local internal efficiency [7]: When bias current I_b goes beyond $I_{th}(x)$ with a photon absorbed at position of x, the energy barrier for a vortex vanishes, leading to the entry of the vortex and to a detection event. Following [7], we posit a relation between local detection efficiency, bias current and threshold current:

$$LDE(x,I_b) = \min[1, \exp((I_b - I_{th}(x))/I^*)] \tag{3}$$

where I_b is the bias current, and I^* is a current scale and it can be extracted from experiments by fitting the internal detection efficiency as a function of I_b. The value of $I^* = 0.65\ \mu$A used in this article is based on the experimental data in [7].

Figure 6 shows the $LDE(x,I_b)$ for several values of I_b up to the critical current I_c, for which we adopt the experimental value of 28 μA [7]. For lower bias currents ($0.7I_c$ and $0.8I_c$) the curves have identical shape but with a different prefactor as expressed by Eq. (3). For low bias currents, the value of the probability at the edges is approximately three orders of magnitude higher than that in the center, which implies that the edges are much more sensitive than the center. Higher current (e.g. $0.9I_c$) leads to saturation of the detection efficiency near the edges and therefore less contrast. At bias currents close to the critical current (I_c) the detector shows a position-independent detection efficiency.

5. Detector response in a scanning probe experiment

An experiment that measures the light count rate as a function of both bias current and tip position can distinguish between the effect of local absorption and the position-dependent internal detection efficiency. In this section we calculate the detector response of an s-SNOM experiment building on the results from the previous sections. We consider a tip that moves across the wire (x direction) with the height of the tip fixed. At each position of the tip we simulate the optical absorption distribution $A(x_{tip},x,y)$ of the nanowire, and then we calculate the integral in Eq. (1) using the position dependent local detection efficiency $LDE(x,I_b)$ at different bias currents from $0.7I_c$ to I_c.

Figure 7 shows the result of the detector response $R(x_{tip},I_b)$ as a function of tip position and bias current for light entering from (a) the $y-$direction (parallel illumination) and (b) the negative $x-$direction (perpendicular illumination). The region without shade represents the location of the nanowire. As a reference, the dashed lines indicate the detector response without tip. In order to facilitate comparison between curves at different bias currents we normalize the calculated $R(x_{tip},I_b)$ as a function of tip position x_{tip} to its maximum value. The whole procedure is repeated for light that is entering parallel and perpendicular to the nanowire.

At lower currents of $0.7I_c$ and $0.8I_c$, the shape of the $R(x_{tip},I_b)$ curves is identical, and the only difference between the two curves is a prefactor of $\sim 10^3$, which is determined by $LDE(I_b,x)$, as shown in Fig. 6. The similarity in shape is a direct result of the assumed scaling

#242194 Received 3 Jun 2015; revised 28 Aug 2015; accepted 2 Sep 2015; published 14 Sep 2015

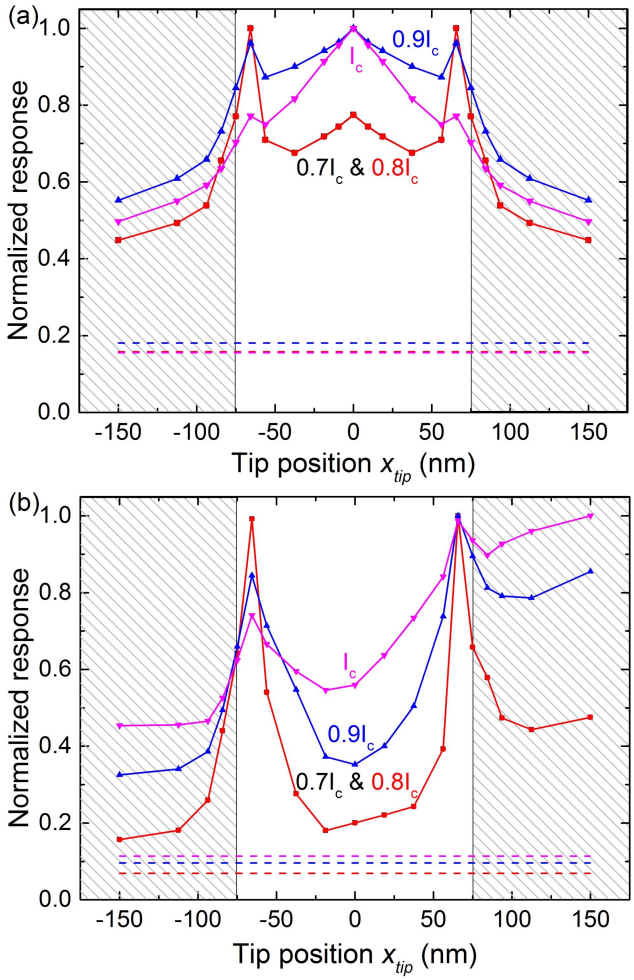

Fig. 7. Detector response as a function of tip position x_{tip} for light incident from (a) the $y-$direction and (b) the $x-$direction. The unshaded area corresponds to the nanowire. The calculation uses the local detection efficiency $LDE(x, I_b)$ in Fig. 6 at several bias currents. The dashed lines (background signal) are the detector response without tip in the system. Each curve is normalized to its maximum value to compare the shape of the response.

#242194 Received 3 Jun 2015; revised 28 Aug 2015; accepted 2 Sep 2015; published 14 Sep 2015

behavior expressed by Eq. (3), and can be verified in a scanning probe experiment at low bias currents. When we consider the higher currents of $0.9I_c$ and I_c, the $LDE(I_b,x)$ first saturates at the edges of the nanowire, leading to differences in the shape of $R(x_{tip},I_b)$.

We note that part of the signal is due to background illumination. In an experiment this background can be distinguished from the signal by varying the tip-detector interaction by modulating techniques [37, 38] that vary the tip-detector distance. The signal of tip-sample (nanowire) interaction depends strongly on the distance to the sample surface while the background of course does not. A modulation of the tip-sample distance with a frequency of Ω will also generate higher order harmonics in the near-field signal. This allows us to demodulate the signal at higher frequencies (e.g. at 2Ω or 3Ω).

The detector response (solid curves in Fig. 7(a)) for parallel illumination shows a symmetric behavior relative to the y-axis, because the illumination parallel to the nanowire (y-axis) makes the incident field symmetric about the y-axis. For smaller bias currents ($0.7I_c$ and $0.8I_c$) the response shows an 'edge effect': The response of the detector has maximum values when the tip moves above the edges of the detector. This edge effect contains a contribution of both the internal detection efficiency and optical absorption that are enhanced at the edge. The internal efficiency is enhanced due to the decrease of the vortex-entry barrier caused by photon absorbed on the edge. The absorption is increased due to the sharpness of the nanowire edge when the tip is above the edge [39]. We find that the absorption (or electric field) is strongly localized within a several nanometers wide area on the edge of the wire (not shown here). The absorption is enhanced in a region ~ 25 nm from the edge for a tip above the edge. The combined effect of the high $LDE(x)$ at the edge and the enhanced absorption near the edge shifts the maximum response towards the edge compared to the maximum absorption.

We observe in Fig. 7 that the response at the lower currents ($0.7I_c$ and $0.8I_c$) does not reach its maximum value when the tip is right above the edge at $x_{tip} = \pm$ 75 nm but when the tip is about 10 nm away from the edge at $x_{tip} \approx \pm$ 65 nm. The position of these maxima is determined by the optical absorption integrated over the detectors, which is maximum when the tip is at $x_{tip} = \pm$ 65 nm. The absorption of the nanowire is determined by two factors. The first factor is the local intensity of the electric field at the tip, which has a maximum value when the point-like source is exactly above the edge ($x_{tip} = \pm$ 75 nm). The second factor is the area of the detector that is exposed to the light from the source, and this area is maximized when the source is right above the center of the detector. The maximum response, when the tip is at $x_{tip} = \pm$ 65 nm, is a tradeoff of these two factors with considering the very high detection efficiency close to the edges.

For higher bias currents ($0.9I_c$ and I_c), the contrast between the edge and the center of the nanowire becomes smaller. When the detector is biased at the critical current I_c the internal efficiency is uniform across the whole detector and the response curve (pink) in Fig. 7(a) at I_c reflects the optical absorption of the detector as a function of tip position.

For all the bias currents the detector response decreases as the tip position is far away from the nanowire. By moving the tip further away we expect the detector response to converge to the background level.

Figure 7(b) shows the detector response where the wave-vector of the incident light is along the x-axis, i.e. perpendicular to the nanowire. There are three differences with the data in Fig. 7(a): 1) The curves are asymmetric about the y-axis with the detector response becoming higher when the tip crosses the nanowire towards the positive x-axis. This is caused by reflected light, which leads to an increase in absorption or response as a function of tip position x. 2) At higher bias currents ($0.9I_c$ and I_c) the response with the tip above the edges is larger than that with the tip above the center of the wire despite the larger absorption area when $x_{tip} = 0$ nm. Similarly to the parallel case, the absorption is localized within a narrow area when the tip is above the

#242194 Received 3 Jun 2015; revised 28 Aug 2015; accepted 2 Sep 2015; published 14 Sep 2015

edges, but the field is more confined in the $x-$direction. As a result a larger response occurs when the tip is above the edges than when the tip is above the center. 3) Compared to the parallel case the contrast of the maximum and minimum value of the response is larger, and the half width of the peaks is narrower ($\sim$ 20 nm). As mentioned in the previous section, the local absorption response in the perpendicular case is similar to that of parallel case but is rotated 90° clockwise, see Fig. 5(a). Hence, when the tip scans over the edge of the nanowire, its localized electric field (with short axis of the absorption area along x-axis) moves from outside into the nanowire with a sharper transition, leading to the larger contrast and narrower response peaks.

In order to experimentally realize the proposed experiment, we discuss several nontrivial details. It is essential to remove the resist layer on top of the NbN nanowire that remains after detector fabrication. Preliminary results show that wet etching in a buffered HF solution can be used and that only $\sim$ 6 nm of HSQ (Hydrogen silsesquioxane) is left on a working NbN nanodetector. The roughness of the NbN plus remaining resist as measured by atomic force microscopy is 1.2 nm (FWHM) and is smaller than the gap of 5 nm and has minimal influence on the optical response.

For the sharp tip, we envisage a configuration similar to that reported in [30], where the gold tip is supported by a silicon pillar. Focused-Ion-Beam (FIB) milling allows fabrication of metal tips with lengths of 200 nm to several tens of micrometers and a radius of curvature of 10 nm at the apex [30]. This tip needs to be illuminated from the side, which we believe can be done using an optical fiber with a graded-index lens which illuminates the detector at a grazing angle of incidence. A choice of a spot-size of 10-100 μm covers the interesting tip-detector region during an approach. The mechanical stage needs to be carefully designed so that a difference in thermal expansion of different materials is compensated for. Ideally, the tip can be coarsely aligned to the detector at room temperature with the help of a CCD camera greatly reducing the problem of positioning the tip above the detector at cryogenic temperatures.

Finally, we note that current crowding effects are present in very short nanowires due to the tapered parts. We have calculated the current distribution in 150 nm wide NbN nanowires of different length. The difference in current density is less than 10% in the nanowire considered here and can be eliminated for nanowires longer than 500 nm.

6. Conclusions

We have numerically investigated a superconducting nanowire single photon detector probed by a near-field, sharp gold tip, which is illuminated by a monochromatic light source. The tip above the detector functions as a nanoscale light source because of the localized electric field at the tip vertex. The tip behaves as a radiative electric dipole due to a surface plasmon resonance and a 'lightning-rod' effect. For a wavelength of 1000 nm, the length of the tip is designed to be 200 nm to create significant resonant enhancement of the local electric field. The absorption of light by the detector is concentrated in an area of 50 nm around the tip, and it is not strongly influenced by the boundary of the wire.

According to a quasiparticle-diffusion and vortex-crossing model we predict that the intrinsic detector response is strongly enhanced near the edges of the nanowire for low bias currents. The detector response is calculated by taking into account this position-dependent local detection efficiency and the position dependence of optical absorption. At high bias currents close to the critical current the internal efficiency is constant and the response of the detector reflects the optical absorption profile when scanning the tip. At lower currents the response curve contains direct information of the intrinsic probability as a function of position. The detection response as a function of tip position exhibits two peaks on the edge of the nanowire due to the distribution of both internal efficiency and optical absorption near the edges. Based on our numerical simulations we estimate that these features can be resolved with a resolution of $\sim$ 20 nm. The

#242194 Received 3 Jun 2015; revised 28 Aug 2015; accepted 2 Sep 2015; published 14 Sep 2015

best resolution is obtained for light incident perpendicular to the wire.

Acknowledgment

This work is funded by the Foundation for Fundamental Research on Matter (FOM), which is financially supported by the Netherlands Organization for Scientific Research (NWO). It is also supported by the Swiss National Science Foundation grant no. 200021_146887/1.

#242194 Received 3 Jun 2015; revised 28 Aug 2015; accepted 2 Sep 2015; published 14 Sep 2015